ACS Sustainable Chemistry & Engineering

Research Article

pubs.acs.org/journal/ascecg

Fabrication of Graphene-Based Xerogels for Removal of Heavy Metal Ions and Capacitive Deionization

Xiaoyu Gu, Yu Yang, Yang Hu, Meng Hu, and Chaoyang Wang*

Research Institute of Materials Science, South China University of Technology, Guangzhou 510640, China

Supporting Information

ABSTRACT: With a rapid increase of population, delivering clean and potable water to humans has been an impending challenge. Here, we report a green method for the preparation of graphene−chitosan−Mn_3O_4 (Gr−Cs−Mn_3O_4) composites, where Gr−Cs hydrogels are first prepared from the self-assembly of chitosan with graphene oxide (GO) nanosheets; then Gr−Cs−Mn_3O_4 composites are obtained by oxidizing Mn(II) ions which are adsorbed by Gr−Cs hydrogels. The effects of pH and mass ratio of GO to Cs on sorption of different ions are investigated. Enhanced capacitive deionization performance of Gr−Cs−Mn_3O_4 composites was also demonstrated. The resultant Gr−Cs−Mn_3O_4 composites exhibit a hierarchical porous structure with a specific surface area of 240 m^2/g and excellent specific capacity of 190 F/g, much higher than those of pristine reduced graphene oxide electrodes. Distinguished electrochemical capacity and low inner resistance endow Gr−Cs−Mn_3O_4 composites with outstanding specific electrosorptive capacity of 12.7 mg/g.

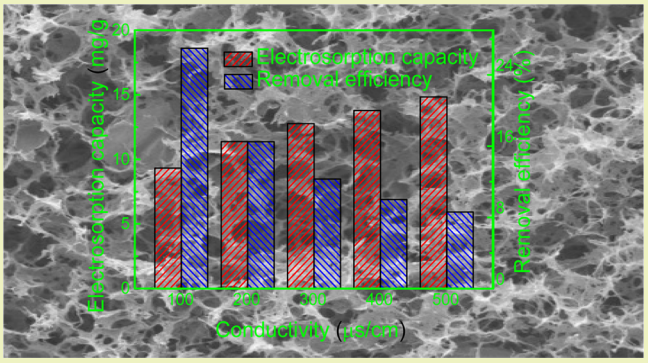

KEYWORDS: *Graphene, Hydrogels, Chitosan, Adsorption, Capacitive deionization*

INTRODUCTION

Water crisis has been one of the most serious problems globally in recent years due to current issues such as population increase, pollution, and global warming. Design and fabrication of new materials, techniques, and devices which can provide safe potable water to humans have been an impending challenge. Desalination of seawater could be a possible solution to this problem, but it is not widely used yet because of the high-power consumption required to make water drinkable. Capacitive deionization (CDI), an electrosorption process to force ionic species toward oppositely charged high-surface-area electrodes under an electric field, is considered as an energy efficient and cost-effective desalination technology.[1] From a fundamental point of view, CDI performance usually depends on the physical and structural properties of the electrode materials such as specific surface, conductivity, and pore size distribution. Relatively high specific surface area (SSA) and better conductivity contribute to a better adsorption capacity.[2] Therefore, it can be said that the majority of effort and focus in CDI research has been put into the development and synthesis of better electrode materials.[3] With its wide variety of available forms and porosity, carbon materials have been found to be the ideal candidates for CDI application.[4] Among the various forms of carbon investigated for CDI, activated carbon,[5] carbon cloth,[6] mesoporous carbon,[7] carbon fiber,[8−10] carbon nanotubes,[11−13] graphene,[14−16] and their composites[17−20] have been studied. Recently, graphene, a new carbon material with one-atom thickness and a two-dimensional plane, has emerged as a key material for designing experimental water treatment strategies owing to their excellent physical, chemical, and electronic properties.[21−27] In particular, graphene/metal oxide composites are drawing increasing attention to electrode materials since graphene not only serves as a highly conductive support material but also provides a large surface for the dispersion of metal oxide nanoparticles.[28−30] Among transition metal oxides, manganese oxide-based electrode materials are one of the most promising electrode materials for commercial supercapacitors because of their good efficiency, better stability, high abundance, and low cost, as well as their different oxidation states of MnO, Mn_3O_4, Mn_2O_3, and MnO_2.[31,32] Furthermore, constructing graphene composite electrodes with manganese oxide can enhance the electronic conductivity of manganese oxide with the aim of improving capacitive performance.[33,34]

Chitosan (Cs), derived from the alkaline deacetylation of chitin, has been intensively studied due to the properties of being environmentally friendly, low cost, and available from an abundant source.[35] Owing to a large amount of primary amines along its backbone, chitosan possesses useful properties including biocompatibility, biodegradability, and antimicrobial ability, especially metal ion adsorption activity.[36] Recently, GO nanosheets were reported as being used as reinforced material

Received: December 2, 2014
Revised: April 27, 2015
Published: May 8, 2015

DOI: 10.1021/acssuschemeng.5b00193
ACS Sustainable Chem. Eng. 2015, 3, 1056−1065

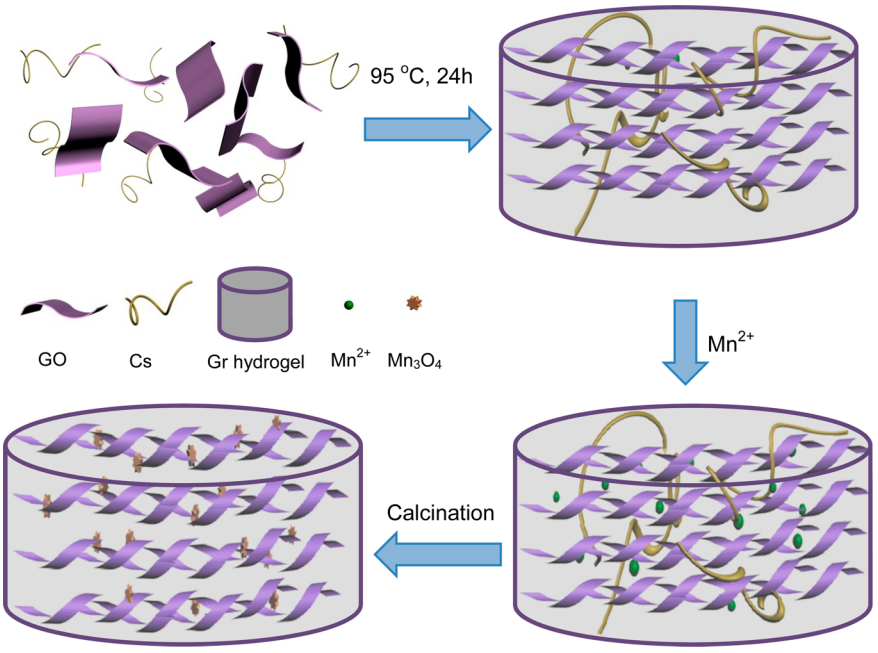

Figure 1. Schematic illustration for the synthesis of Gr−Cs and Gr−Cs−Mn_3O_4 xerogels.

to blend with chitosan for nanocomposite preparation.[37] In fact, the inherent chemical structures of GO and CS have the potential for cross-linking reactions similar to the curing of epoxy resin because GO bears with epoxy groups and Cs has amino groups.[38] Additionally, the introducing chitosan can minimize the restacking effects of graphene sheets as "spacers" since dried graphene nanosheets naturally aggregate and stack to multilayers, inducing inferior physical and chemical properties than that in their exfoliated monolayer state.[28,39] In view of favorable adsorption properties of chitosan and inherent properties of graphene oxide (GO), the composites coupling of graphene with chitosan can boost the adsorption capacity and electrochemical properties.[40,41]

Here, we report a facile preparation of hierarchical graphene−Cs (Gr−Cs) and Gr−Cs−Mn_3O_4 xerogels based on graphene and chitosan for multiple water treatments. On the one hand, Gr−Cs xerogels have high sorption capacity in the preconcentration of heavy metal ions because of the functional groups on the graphene and chitosan surfaces. On the other hand, owing to the synergistic effect from a combination of metal oxide materials and conductive graphene networks, the as-prepared Gr−Cs−Mn_3O_4 xerogels as working electrodes show enhanced specific capacitance in electrochemical performance and outstanding specific electrosorptive capacity of CDI performance. The route for the synthesis of Gr−Cs−Mn_3O_4 composites mainly involved three steps: (1) Hydrogels of graphene−chitosan (Gr−Cs) were prepared by noncovalent interactions. (2) The Gr−Cs xerogels had high adsorption toward different heavy metal ions, including Mn(II), Pb(II), and Ni(II). (3) With the aid of high-temperature processing, Mn(II) ions were transformed to active materials Mn_3O_4, and finally Gr−Cs−Mn_3O_4 xerogels were obtained. The detailed preparation process of 3D graphene-based xerogels is shown in Figure 1.

EXPERIMENTAL SECTION

Materials. Natural graphite powder was purchased from J&K Scientific Ltd. (China). Chitosan with a degree of deacetylation ≥90.0% and a viscosity average molecular weight of 6×10^4 was purchased from Shanghai Bo'ao Biological Technology Co. Ltd. (China). Manganese sulfate ($MnSO_4$), lead nitrate ($Pb(NO_3)_2$), and nickel chloride ($NiCl_2$) were purchased from Aladdin Reagent Co. Ltd. (China). All other reagents were purchased from Guangzhou Chemical Reagent Co. (China) and used without further purification. Water used in all experiments was deionized and filtrated by a Millipore purification apparatus with a resistivity of more than 18.0 MΩ·cm.

Preparation of Gr−Cs Hydrogels and Xerogels. GO was prepared from purified natural graphite via the modified Hummer's method, and the corresponding details can be obtained in our previous report.[42] Homogeneous suspension of GO (4 mg/mL) was obtained after the product was ultrasonicated for 2 h in deionized water. In order to obtain 2.0 wt % chitosan aqueous solutions, 2 g of chitosan powder was dissolved in 200 mL of glacial acetic acid solution (2.5 wt %) and stirred overnight. It is well-known that gelation occurs immediately when GO and chitosan solutions are put together under acidic conditions, leading to a sharp increase in the viscosity. Thus, slight inhomogeneity of the hydrogel is inevitable if GO and chitosan solution are direct mixed.[43] So the pH values of GO solution were adjusted to 10 by the addition of 1 M NaOH solution to hinder the formation of the hydrogel when GO and CS were mixed. Then different amounts of chitosan solutions were added dropwise to the GO suspension to make the GO/Cs mass ratio change from 5:1 to 10:1 to 20:1. Stable hydrogels can be formed by adding a glacial acetic acid solution into the mixed viscous solution, because of the decrease of the amount of negative charge as well as electrostatic repulsion between GO sheets and chitosan. Finally, the above mixtures were heated to 90 °C for over 24 h to form the Gr−Cs hydrogels. The resulting hydrogel was freeze-dried by a vacuum freeze-dryer to maintain the porous structure. For convenience, the samples are denoted by Gr−Cs_n where subscript n represents the mass ratio of GO to chitosan. Unless specifically noted, Gr−Cs refers to Gr−Cs_{10}.

Preparation of Gr−Cs−Mn_3O_4 Xerogels. The obtained Gr−Cs hydrogel was immersed in the heavy metal ion solution (1 mmol/L) and continuously stirred for 24 h to ensure full adsorption. Then the Gr−Cs hydrogels whose networks were full of metal ions were freeze-dried by a vacuum freeze-dryer again. Finally, the above composites were annealed at 700 °C for 7 h under a N_2 atmosphere with a heating rate of 4 °C/min in a tubular furnace. After high-temperature processing, chitosans within the composite were calcined into carbon

DOI: 10.1021/acssuschemeng.5b00193
ACS Sustainable Chem. Eng. 2015, 3, 1056−1065

phase and manganese ions were transferred to Mn_3O_4, so as to get the Gr−Cs−Mn_3O_4 composites. For comparison, Gr−Cs−PbO and Gr−Cs−NiO composites were prepared in the same route using $Pb(NO3)_2$ and $NiCl_2$ instead of $MnSO_4$. Pristine Gr hydrogels were also prepared according to the above procedure in the absence of chitosan and metal ions.

Adsorption Experiments. To measure the adsorption capacities of GO−Cs xerogels, 50 mg of xerogels was immersed into 100 mL pollutant solution containing metal ions. The amounts of metal ions adsorbed on Gr−Cs xerogels were calculated from the difference between the initial concentration (ϕ_0) and the equilibrium one (ϕ_e). The adsorption capacities of the xerogels toward different adsorbates can be adjusted by changing the GO/Cs mass ratio of the xerogels. The amount of adsorption σ (mmol/g) was calculated according to the following equation:

$$\sigma = \frac{(\phi_0 - \phi_e)\upsilon}{\omega} \quad (1)$$

where ϕ_0 and ϕ_e (mg/L) are the initial and final Mn(II) ion concentrations, ν (L) is the volume of the Mn(II) ion solution, and ω (g) is the weight of the dried Gr−Cs xerogels.

Electrochemical Measurements. The working electrode was prepared by pressing a paste of Gr−Cs−Mn_3O_4 xerogels (80 wt %), acetylene black (10 wt %), and polytetrafluoroethylene (10 wt %) onto a nickel foam plate. Before casting and pressing, the raw mixture was ground for several hours to increase its homogeneity. A three-electrode cell system, including a graphene-based electrode, Pt foil, and Ag/AgCl (3 M KCl) were used as the working, counter, and reference electrodes. All of the experiments were carried out in 1 M NaCl aqueous electrolyte.

Cyclic voltammetry (CV) analysis of graphene-based electrodes was measured using an electrochemical workstation (CHI660C instruments, Shanghai, China). The potential range for CV was −0.6−0.4 V, and the effects of changes in the scan rate were examined by supplying 5, 10, 20, and 50 mV/s.

The galvanostatic charge/discharge (GC) tests were conducted on an automatic LAND battery test instrument (CT2001A) to evaluate the charge−discharge performance in 1 M NaCl aqueous solution. Here, the specific capacitances Cs were calculated from the slope of discharge curves by using the following equation:

$$C_s = \frac{I\Delta t}{m\Delta V} \quad (2)$$

where C_s (F/g) is the specific capacitance, I (A) is the constant discharge current, Δt (s) is the discharging time, m (g) is the mass of working electrode in milligram scale, and ΔV is the voltage drop upon discharging (excluding the iR drop).

Electrochemical impedance spectroscopy (EIS) measurements were also measured by CHI 660C. The amplitude of the alternating voltage was 5 mV around the equilibrium potential (0 V) and the data was collected in the frequency range from 100 mHz to 100 kHz.

Electrosorptive Capacity Measurement. Graphite papers were used as inert current collectors on the back sides of the electrodes, and the working electrodes were prepared in the same manner as above in electrochemical measurements. The size of the electrode was 40 × 40 mm, and each electrode mass was 0.1 g. A flow channel was created by punching a 1 cm diameter hole in the graphite sheet so that the solution could be in contact with all sides of the working electrodes and could run through the spacer to the outer reservoir (Scheme S1). The electrosorptive capacity of the graphene-based electrode was conducted in a recirculating system including an electrosorptive unit cell and conductivity monitor as shown in Scheme S1; details of the apparatus and experimental procedures were described elsewhere.[44] The system consisted of a reservoir, a peristaltic pump (BT-100), the CDI device, and a conductivity meter. A given potential of 1.6 V was applied to the CDI cell using a potentiostat (RS1302DQ). The conductivity of the effluent water was measured by connecting a conductivity meter (DDS 307) at the position where the solution exited the cell. NaCl solution with an initial conductivity in a total volume of 150 mL was continuously pumped into the unit cell by a peristaltic pump with a flow rate of 10 mL/min to the feed tank. The relationship between conductivity and concentration of NaCl solution can be found in Figure S1. Herein, the electrosorptive capacity (q_e, mg/g) of current electrodes was calculated according to the following equation:[45]

$$q_e = \frac{(C_0 - C_e)V}{m} \quad (3)$$

where C_0 (mg/mL) and C_e (mg/mL) are the initial and equilibrated NaCl concentrations, respectively, V (mL) is the volume of the container, and m (g) is the mass of active components in two working electrodes.

Characterization. The concentrations of metal ions left in solution were determined by atomic absorption spectroscopy (AAS Hitachi Z200). The morphology of Gr−Cs hydrogels was examined by scanning electron microscopy (SEM Zeiss EVO18) operating at 10 kV, all samples were sputter-coated with a thin overlayer of gold to prevent sample charging effects. The X-ray diffraction (XRD) patterns of pristine Gr hydrogel and Gr−Cs−Mn_3O_4 composites were obtained using an X'pert PRO diffractometer (40 kV and 40 mA) equipped with a Cu Kα radiation (wavelength 0.154 nm) at room temperature. FT-IR spectra were obtained on an FT-IR NICOLET 6700 spectrometer at a nominal resolution of 2 cm^{-1}. Theta probe x-ray photoelectron spectroscopy (XPS, ESCA Axis Ultra DLD) was used to verify the valence state of carbon and nitrogen. The Brunauer−Emmett−Teller (BET) method was utilized to calculate the specific surface area. The pore size distributions were derived from the desorption branch by using the Barrett−Joyner−Halenda (BJH) model. Before the measurements, all samples were degassed overnight at 373 K in a vacuum line.

RESULTS AND DISCUSSION

Fabrication of Gr−Cs and Gr−Cs−Mn_3O_4 Xerogels. Gr−Cs composite hydrogels and xerogels can be easily formed by directly mixing GO aqueous dispersion and Cs solution due to the epoxy groups on the GO sheets and amino groups on the chitosan (Figure S2a,b).[46] After adjusting to alkaline, a large number of reactive groups, like −COOH, −OH, and so forth on the surface of GO sheets, could be neutralized by NaOH.[47] Therefore, the formation of the hydrogel was hindered when GO and Cs mixed. However, electrostatic repulsion between GO sheets decreased with the addition of acid solution, as well as gelation came into being. After heating at 90 °C for over 24 h, 3D graphene networks were formed by hydrothermal reduction of GO sheets in their aqueous dispersion, owing to the partial overlapping or coalescing of flexible graphene sheets via $\pi-\pi$ stacking interactions.[48] Figure S2c shows the Gr−Cs_n (n = 5, 10, 20) hydrogels with a different mass ratio of GO to Cs. We can find that the volume of Gr−Cs hydrogel became smaller when the amount of chitosan in GO was less. It is because that chitosan within the hydrogel would prevent $\pi-\pi$ stacking interactions of graphene sheets. After being dried by a vacuum freeze-dryer, the lyophilized Gr−Cs hydrogel was obtained and used to absorb metal ions. As shown in Figure S2d and S2e, the shrinkage of Gr−Cs was not obviously compared with the cylindrical vessels. TG curves of Gr, Gr−Cs_{10}, Gr−Cs−$MnCl_2$, and Gr−Cs−Mn_3O_4 composites are shown in Figure S3. The residual weight of Gr−Cs−Mn_3O_4 composites was 96% due to sufficient calcination. With the increasing addition of chitosan and $MnCl_2$, the residual weight of Gr, Gr−Cs_{10}, and Gr−Cs−$MnCl_2$ gradually increased, which confirmed that chitosan and $MnCl_2$ were uniformly distributed in the graphene sheets.

Table 1 shows the adsorption capacity of Gr−Cs_n xerogels with a different mass ratio of GO to Cs in various pH value

DOI: 10.1021/acssuschemeng.5b00193
ACS Sustainable Chem. Eng. 2015, 3, 1056−1065

Table 1. Adsorption Capacity of Gr−Cs Xerogels toward Different Metal Ions at Various pH Values[a]

sample	Mn(II) pH = 4	Mn(II) pH = 6	Mn(II) pH = 8	Pb(II) pH = 6	Ni(II) pH = 6
Gr−Cs_5	0.58	0.8	1.38	1.14	0.58
Gr−Cs_{10}	0.64	0.84	1.46	1.22	0.62
Gr−Cs_{20}	0.68	0.88	1.58	1.4	0.84

[a]The unit of all adsorption capacity is mmol/g.

solutions. Herein, three metal ions, Mn(II), Pb(II), and Ni(II), were chosen to investigate the adsorption performance experiment. At a pH of 6, the adsorption capacity of Mn(II) increased with the GO content, from 0.8 mmol/g for GO−Cs_5 to 0.84 and 0.88 mmol/g for GO−Cs_{10} and GO−Cs_{20}, respectively. The same phenomenon also can be found in the adsorption experiment of Pb(II) and Ni(II). It indicates that GO is a better absorbent for Mn(II) compared with chitosan. It is well-known that both GO and Cs are good absorbents for metal ions,[40,49−51] but the positive metal ions are more difficult to adsorb on the positively charged chitosan surface because of the electrostatic repulsion.[43] However, to the best of our knowledge, the adsorption capacities are comparable with the reported values of GO and Cs, which can attribute to the coordination of both GO and CS with metal ions. The pH of the aqueous solution is an important parameter to determine metal adsorption capacity onto Gr−Cs hydrogel. As shown in Table 1, the adsorption capacity of GO−Cs_{10} for Mn(II) at pH = 8 (1.46 mmol/g) is much larger than that of pH = 4 (0.64 mmol/g) and pH = 6 (0.84 mmol/g). GO−Cs_5 and GO−Cs_{20} composites showed the same adsorption capacity change as pH increase. The increase of pH of the chemical environment caused the deprotonation of the oxygen-containing acidic groups in the Gr−Cs composites, and the amino groups of chitosan were not protonated, which established a negative surface charge density.[52] Therefore, at a higher pH, the nitrogen and oxygen atoms of chitosan, as well as plenty of oxygen atoms on GO, produced stronger electrostatic interactions between metal ions and Gr−Cs composites.[53] In Table 1, the adsorption capacity of the Gr−Cs_{10} composite for Mn(II), Pb(II), and Ni(II) at pH = 6 are 0.84, 1.22, and 0.62 mmol/g, respectively. These data revealed that the Gr−Cs_{10} composite was a suitable absorbent for Pb(II) compared with Mn(II) and Ni(II). Actually, Pb(II) ions have a higher electronegativity and a larger ionic radius than Mn(II) and Ni(II); thus the affinity between Pb(II) and the Gr−Cs_{10} composite is larger than that of Mn(II) and Ni(II). Therefore, the adsorption capacity of Pb(II) was higher than that of Mn(II) and Ni(II) ions. In general, all results in Table 1 prove that GO−Cs xerogels are suitable materials for various types of heavy metal ion pollution cleanup.

Owing to the $\pi-\pi$ stacking between graphene sheets, 3D graphene networks were formed in lyophilized Gr xerogel by hydrothermal reduction of GO sheets in their aqueous dispersion. As shown in Figure 2a, the Gr xerogels have the interconnected network with the porous structure, and the pores range from submicrometers to several micrometers. Figure S4 shows a typical AFM image of single sheets of prepared Gr. The average thickness of the Gr sheets was about 1 ± 0.5 nm, which indicated two or three layers. More detailed information on Gr can be found in the TEM image of Figure S5a. Figure 2b shows that the 3D porous structure of Gr−Cs hydrogels is maintained well with a slightly increased wall thickness due to the chitosan covering. The noncovalent interactions between chitosan and GO are the driving force for the formation of the supramolecular structures.[43] As we can see, the pores in the Gr−Cs hydrogel are dozens of micrometers in size, much larger than that of pristine Gr hydrogel. This unique 3D morphology and chitosan sheets effectively prevent restacking of graphene sheets, which can offer open a diffusion path for the efficient access of both charge and metal ions. As shown in Figure 2c and d, a lot of nanosize nanoparticles are distributed on the graphene sheets of Gr−Cs−Mn_3O_4 hybrid composites. Graphene sheets with nanoparticles are more clearly shown in TEM images of Figure S5b,c. Figure S6 is the corresponding EDS mapping of C, O, and Mn elements. Manganese elements were uniformly distributed in Gr−Cs−Mn_3O_4 composites, providing evidence for successful manganese doping. It further proved that the hybrid Gr−Cs−Mn_3O_4 composites were successfully fabricated by direct absorption of metal ions which were transformed to metal oxide materials after annealing at 700 °C.

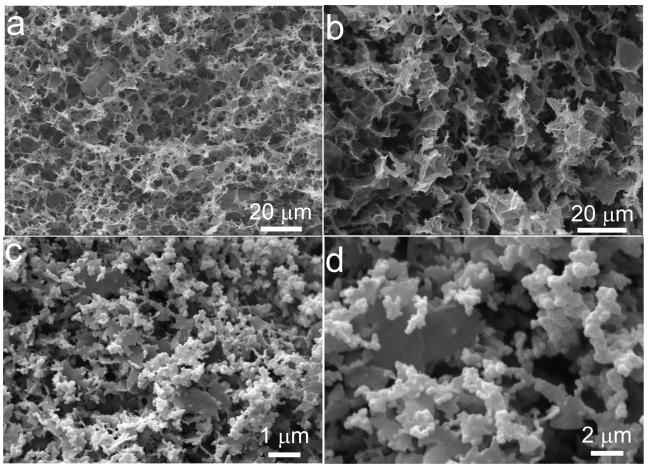

Figure 2. SEM images of (a) lyophilized Gr and (b) Gr−Cs. (c,d) Gr−Cs−Mn_3O_4 xerogels.

The element composition and surface chemical status were carried out by XPS on the GO, Gr and Gr−Cs−Mn_3O_4 composites. Figure 3a shows the wide survey scans of the XPS spectra of all samples. There is only a C 1s peak and very weak O 1s peak of Gr, and the intensities of the O 1s peak are much smaller than those in GO, consistent with reduction of GO. From the XPS spectra of Gr−Cs−Mn_3O_4, we can observe a manganese oxidation state from the multiplet splitting of the Mn 3s and Mn 2p peak. In the Mn 2p region, a 2p3/2−2p1/2 doublet at 651.0 and 639.3 eV is shown in Figure 3b, and the splitting width is 11.7 eV. In the Mn 3s region, the splitting width is 5.4 eV (Figure 3c), which is in agreement with an earlier report on Mn_3O_4.[54] Additionally, more detailed information on the XPS spectra of Gr−Cs−NiO and Gr−Cs−PbO is shown in Figure S7.

To further clarify the structures of the composites, XRD experiments were carried out. As depicted in Figure 3d, all of the diffraction peaks in the XRD patterns exhibit a strong intense (002) peak at $2\theta = 25°$ and no (001) peak at 10.3°, indicating that most of the oxygen-containing groups on basal planes of the carbon networks have been removed. Furthermore, we can find that all the Gr−Cs composites

DOI: 10.1021/acssuschemeng.5b00193
ACS Sustainable Chem. Eng. 2015, 3, 1056−1065

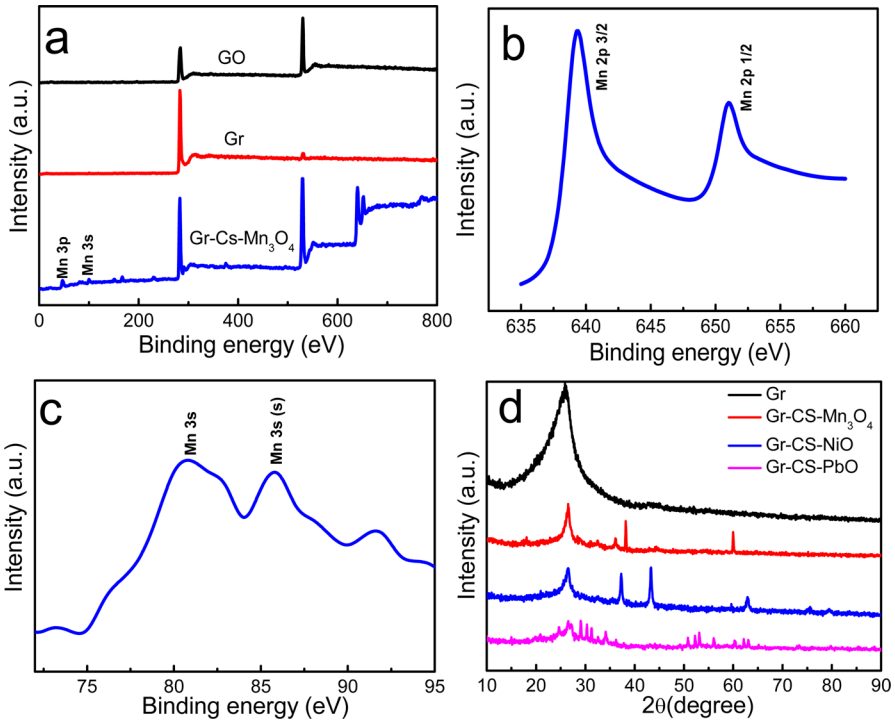

Figure 3. (a) Wide survey scans of the XPS spectra of GO, Gr, and Gr−Cs−Mn_3O_4 composites; (b) XPS spectra of Mn 2p peaks and (c) Mn 3s peaks of Gr−Cs−Mn_3O_4 composite. (d) XRD patterns of Gr, Gr−Cs−Mn_3O_4, Gr−Cs−NiO, and Gr−Cs−PbO composites.

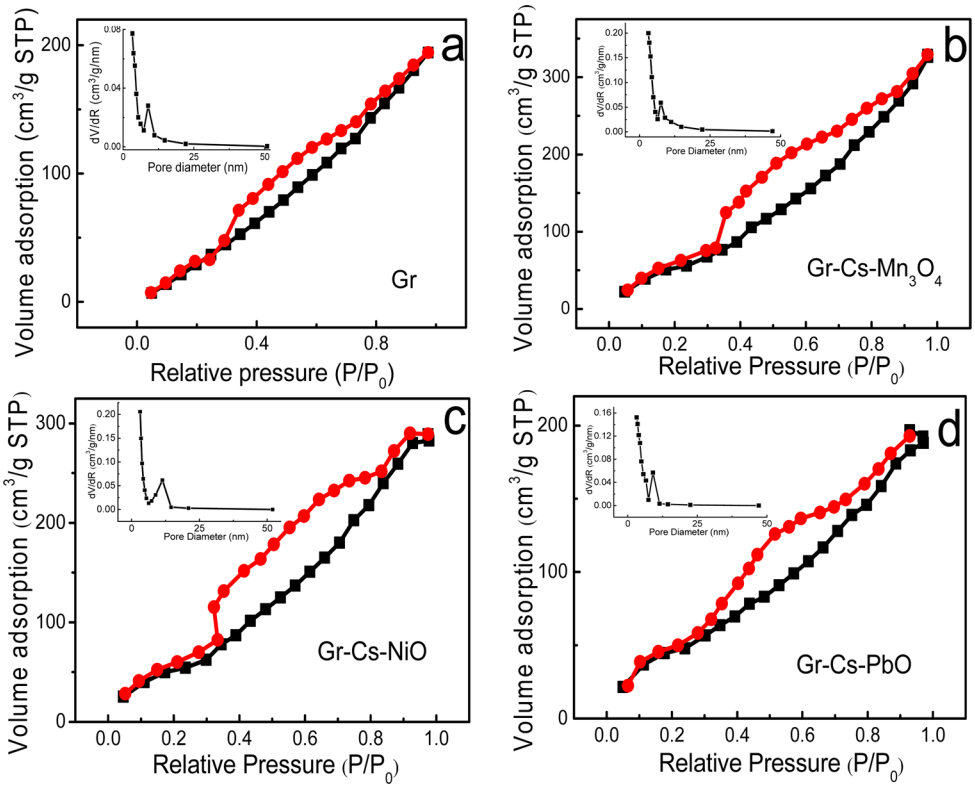

Figure 4. Nitrogen sorption isotherms and pore size distribution (inset) of (a) Gr, (b) Gr−Cs−Mn_3O_4, (c) Gr−Cs-NiO, and (d) Gr−Cs-PbO.

show a similar XRD pattern to the pristine Gr except the peaks of metal oxide, which means that the introduction of chitosan had no significant effect on the macroporous network of Gr−Cs composites. It can be seen that the peaks at 28.9°, 36.1°, 38.1°, 44.7°, and 60° in the Gr−Cs−Mn_3O_4 composites can be indexed to Mn_3O_4, which are in good agreement with the reported values in JCPDS card (018−0803).[55] Furthermore, different metal ions, like Pb(II) and Ni(II), were also absorbed by Gr−Cs hydrogels and transformed to metal oxide. The characteristic peaks at 2θ around 37°, 43°, and 62° appear in

DOI: 10.1021/acssuschemeng.5b00193
ACS Sustainable Chem. Eng. 2015, 3, 1056−1065

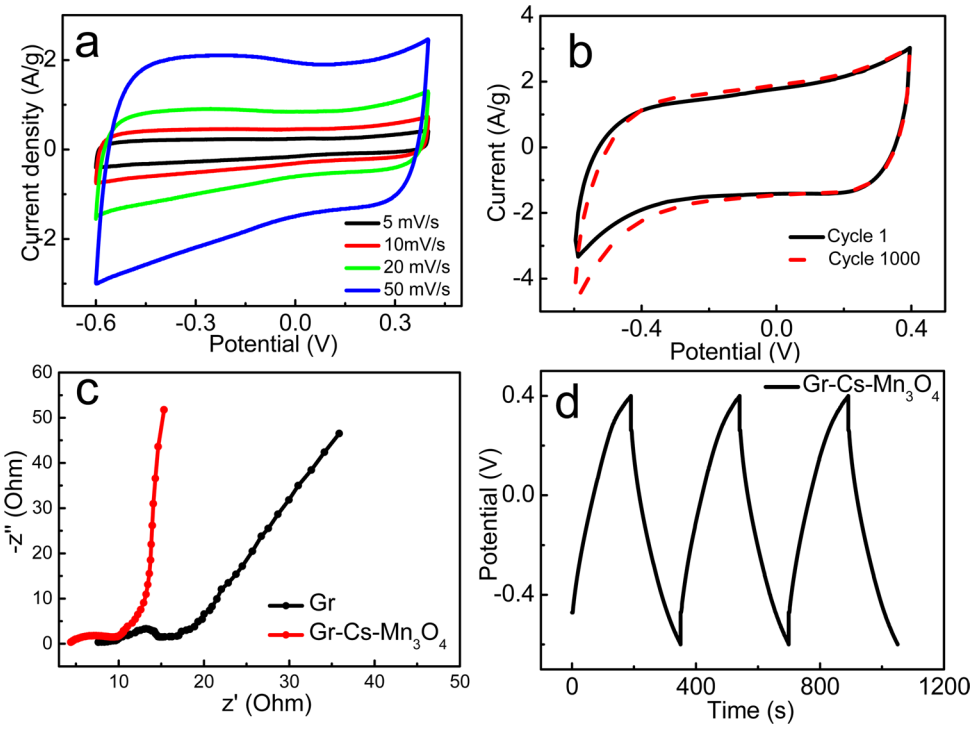

Figure 5. CV curves of Gr−Cs−Mn_3O_4 electrodes (a) at various scan rates and (b) at a scan rate of 50 mV/s during 1000 cycles. (c) Nyquist plots of the EIS for Gr and Gr−Cs−Mn_3O_4 electrodes. (d) GC curves at a current of 1 A/g of Gr−Cs−Mn_3O_4 electrodes.

Gr−Cs−NiO hybrid composites, which are attributed to diffraction from the (101), (012), (110), (113), and (202) planes (JCPDS 044−1159).[56,57] The diffraction peaks at 30.5°, 31.3°, 32.5°, 34.2°, 49.2°, 53.2°, and 60.2° in Gr−Cs−PbO composites are consistent with the JCPDS (005-0570) of PbO.[58] More detailed information is also confirmed by the FT-IR observations (Figure S8).

Large specific surface area and suitable pore size distribution is crucial for electrode materials. As shown in Figure 4, the isotherms of all tested materials can be classified as type IV with a typical H3 hysteresis loop. A slight increase of adsorption at low relative pressure indicates some microspores in the material, while the hysteresis loops at relative pressures above 0.4 clearly show the presence of mesoporosity. The adsorption curves further increase at relative pressure close to unity, indicating the presence of large interparticle voids. It can be concluded that this sample contains macropores together with the mesopores, in which macropores are resulting from the removal of chitosan and mesopores are attributed to the gas release through the high-temperature calcination process. The BET specific surface area of Gr−Cs−Mn_3O_4 is measured to be 240 m^2/g (Figure 4b), which is much higher than that of Gr (120 m^2/g, Figure 4a). The high specific surface area of Gr−Cs−Mn_3O_4 is due to the incorporation of chitosan effectively prevents the aggregation of individual graphene sheets during the thermal treatment. As shown in Figure 4c and d, Gr−Cs−NiO and Gr−Cs−PbO have a specific surface area of 210 and 165 m^2/g, respectively. The values are smaller than that of Gr−Cs−Mn_3O_4 but still larger than that of Gr hydrogel. The BET surface area, pore volumes, and average pore size of all samples are shown in Table S2. These results demonstrate that the Gr−Cs annealing strategy is an efficient way to obtain a graphene electrode with enlarged specific surface area and a wide pore size distribution.

Electrochemical Performance. To investigate the performance of Gr−Cs−Mn_3O_4 as electrodes, various electrochemical measurements were performed. Cycle voltammetry (CV) was first carried out in a three electrode system to evaluate the electrosorption ability of Gr−Cs−Mn_3O_4 composites. Figure 5a displays CV curves of Gr−Cs−Mn_3O_4 at different scan rates from 5 to 50 mV/s in 1 M NaCl aqueous solution. When the scanning rate increases from 5 to 50 mV/s, the current density response increases accordingly. No significant change in the shape of the CV curve can be observed, indicating the good rate property of the Gr−Cs−Mn_3O_4 composite electrode.[59] However, the Gr electrode displayed an increased distortion from the typical rectangular shape with the increase of scan rate (Figure S9a). Compared to the pristine Gr, the Gr−Cs−Mn_3O_4 electrode shows a larger CV enclosed area, which indicates larger specific capacitance and better electrosorption performance. These values agree well with the higher surface area observed for Gr−Cs−Mn_3O_4, which undoubtedly facilitates the adsorption of the ionic species.[60] The superior electrochemical properties of Gr−Cs−Mn_3O_4 hybrids are also highlighted by their excellent cyclic stability. Figure 5b shows the CV curves of Gr−Cs−Mn_3O_4 electrodes at a scan rate of 50 mV/s during 1000 cycles. We can find that their CV curves keep the original shapes with a little change after 1000 cycles. The satisfied electrochemical stability should be attributed to the high electroactive regions and short diffusion lengths provided by stable 3D structures of the Gr−Cs−Mn_3O_4 network.[61]

The Nyquist plots for the Gr and Gr−Cs−Mn_3O_4 electrodes are displayed in Figure 5c. The Nyquist plot shows two regions between Z' (impedance axis) and $-Z''$ (real axis) appeared with the semicircle and nearly vertical lines in the high and low frequency zones, respectively. The intercept of the semicircle on the real axis at high frequency represents the equivalent series resistance (Rs). The Rs value of Gr−Cs−Mn_3O_4 is

DOI: 10.1021/acssuschemeng.5b00193
ACS Sustainable Chem. Eng. 2015, 3, 1056−1065

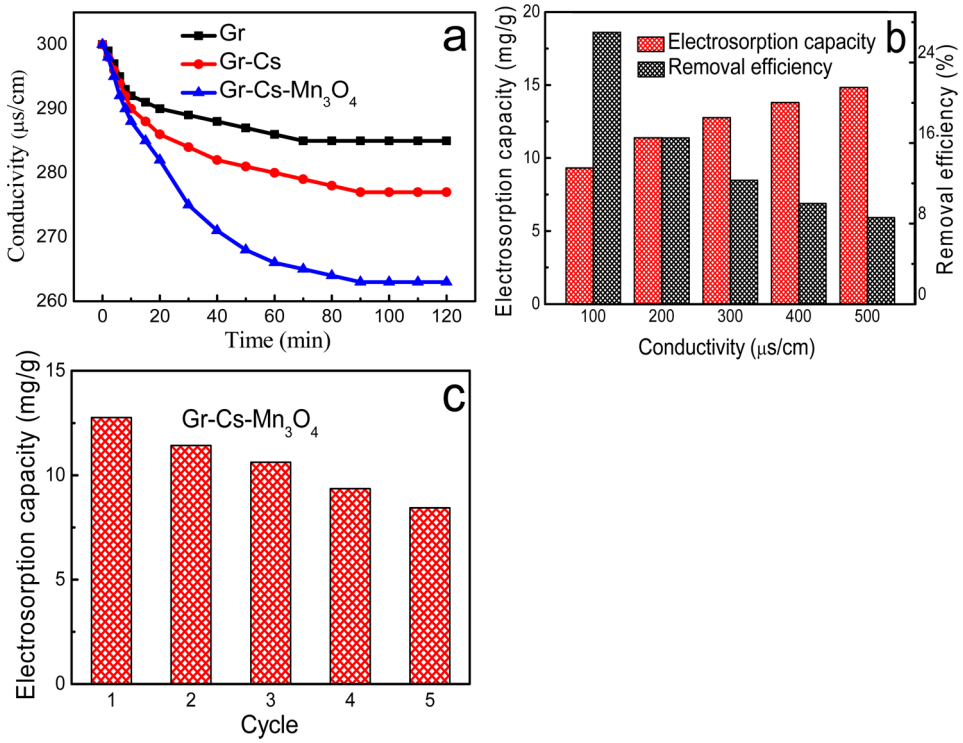

Figure 6. (a) CDI profiles of Gr, Gr−Cs, and Gr−Cs−Mn_3O_4 electrodes under 1.6 V. (b) Electrosorption capacity and removal efficiency of Gr−Cs−Mn_3O_4 electrode in NaCl solutions with respect to different initial concentrations. (c) Regenerated electrosorptive capacity of Gr−Cs−Mn_3O_4 electrode.

smaller than that of Gr, which makes a negligible contribution to the overall electrode resistance. In the high frequency region, the diameter of the semicircle corresponds to the charge transfer resistance (Rct), which can be measured by the impedance axis.[62] As shown in Figure 5c, the Gr−Cs−Mn_3O_4 electrode has a lower transmission resistance than the Gr, suggesting the decreased limitation of the electrochemical reaction. At the low-frequency region, a more vertical straight line is evident for the Gr−Cs−Mn_3O_4 electrode than for the Gr sample, which indicates the faster ion diffusion behavior of the Gr−Cs−Mn_3O_4 electrode.[46]

As shown in Figure 5d, the GC curves of all electrodes display symmetric and linear shapes with a low potential drop (*iR* drop), indicating that Gr−Cs−Mn_3O_4 electrodes exhibit good stability in repeat charge−discharge processes. According to eq 1, the Cs of Gr−Cs−Mn_3O_4 is 190 F/g, larger than that of Gr because of the longer discharge time. Generally, the Cs is an effective parameter to investigate the performance of the CDI electrode material. Therefore, it implies that the Gr−Cs−Mn_3O_4 composites with a higher specific capacitance and better cyclability and stability would enhance desalination efficiency by the incorporated materials. The key to the high electrochemical performance of this hybrid can be ascribed to two reasons: On the one hand, the hierarchical pore structure prepared from the self-assembly of chitosan chains with GO nanosheets can facilitate ion diffusion during the electrochemical procedure. On the other hand, intercalated Mn_3O_4 during graphene synthesis has a great impact on enhancing the energy density through optimizing the ion accumulation into graphene sheets. In conclusion, the Gr−Cs−Mn_3O_4 composites exhibit excellent electrochemical capacity with low inner resistance and high reversibility because of the synergistic effect of the high capacitance of Mn_3O_4 coating and the porous structure of Gr−Cs network.

CDI Performance. Desalination performances of the fabricated electrodes were investigated by batch mode experiments which were conducted in NaCl solutions with various initial concentrations at a working voltage of 1.6 V. The potential difference given herein exceeded the 1.23 V threshold to compensate for the circuit system resistance, and hence no hydrolysis happens in these cases.[3] As shown in Figure 6a, the solution conductivity of all electrodes decreased correspondingly with the operating time, which demonstrated quick adsorption of the salt ions after the voltage was applied. Apparently, the Gr−Cs−Mn_3O_4 electrodes performed faster and had a higher adsorption amount compared to pristine Gr and Gr−Cs electrodes because of easy surface accessibility for ion adsorption from the saline solution to the electrode surface. According to eq 3, the electrosorptive capacity of 12.7 mg/g for Gr−Cs−Mn_3O_4 was obtained, much higher than 6.5 mg/g for Gr and 7.93 mg/g for Gr−Cs electrodes. This result shows that Gr−Cs−Mn_3O_4 with higher SSA and enhanced specific capacitance has the higher electrosorption capacity. This tremendous improvement in the salt removal can be attributed to good incorporation and low agglomeration of chitosan and Mn_3O_4 into graphene sheets.

As shown in Figure 6b, the total capacity increase but salt removal efficiency decrease as the ion solution concentrations increase. The electrosorptive capacities are 9.32, 11.38, 12.76, 13.79, and 14.83 mg/g as the initial concentrations of the NaCl solutions are 100, 200, 300, 400, and 500 μs/cm, whereas the salt removal rates are 27, 16.5, 12.3, 10%, and 8.6%, respectively. It is obvious that the higher initial concentration of solution is, the larger the adsorption capacity that can be obtained at equilibrium. This is because the overlapping effect

DOI: 10.1021/acssuschemeng.5b00193
ACS Sustainable Chem. Eng. 2015, 3, 1056−1065

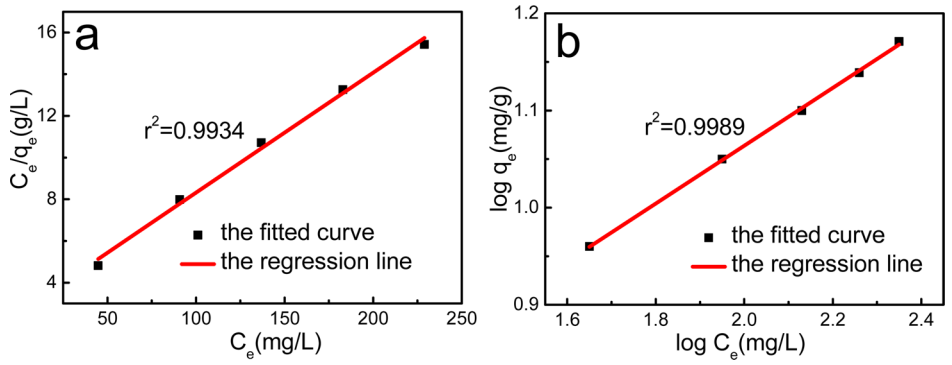

Figure 7. Fitting regression line by (a) Langmuir and (b) Freundlich equation for the electrosorptison of Gr−Cs−Mn_3O_4 electrodes.

of the electrical double layer on the micropores decreases at higher salt concentrations.[63] However, when the concentration of NaCl exceeds a certain value, the absolute increased number of ions in solution is far larger than the amount of the adsorbed ones, which results in the declines of adsorption rate contrariwise. In fact, the electrical double layer thickness is inversely proportional to the solution concentration. Therefore, with a lower concentration, the electric field can extend to a longer distance since the solution is less effective in holding the charge.[64] It brings the phenomenon that the higher initial concentration of NaCl solution is, the worse the salt removal efficiency becomes.

Good regeneration performance of the utilized electrodes is an important parameter for ensuring the future long life of the CDI cell. Figure 6c shows the regenerated electrosorptive capacity of the Gr−Cs−Mn_3O_4 electrode, and the electrosorptive capacities are 12.7, 11.4, 10.6, 9.3, and 8.4 mg/g from the first to fifth time. It is noteworthy that Gr−Cs−Mn_3O_4 electrodes could be regenerated very well just by turning off the cell voltage, confirming that the CDI is an energy efficient desalination technology without secondary pollution, which is critical for large scale application. The decrease of regenerated electrosorptive capacity of Gr−Cs−Mn_3O_4 can be ascribed to two reasons: (1) Ions of opposite charge can simultaneously move toward the electrode from the bulk solution after Gr−Cs−Mn_3O_4 electrodes were regenerated by turning off the cell voltage. As a result, all adsorbed ions were not desorbed from the Gr−Cs−Mn_3O_4 electrode surface, and a portion remained inside the porous graphene electrode.[65] (2) During cycles, Faradaic reactions between functional groups such as carbonyl and phenolic groups on the carbon electrode and cations also decreased the active sites on the electrodes for ion adsorption.[66] Therefore, due to the limited ion adsorption capacity of the electrode, the number of ions that are adsorbed to the electrode gradually deceases during the operation cycle.[67]

To investigate the electrosorption behavior, we use the classical Langmuir and Freundlich models to fit the curve of the Gr−Cs−Mn_3O_4 electrosorption isotherm of NaCl solution with various initial concentrations, as shown in Figure 7. Here the Langmuir and Freundlich models can be predigested as

$$\text{Langmuir: } q_e = \frac{q_m K_L C_e}{1 + K_L C_e} \tag{4}$$

The linear form of the Langmuir model could be expressed as

$$\frac{C_e}{q_e} = \frac{1}{q_m K_L} + \frac{C_e}{q_m} \tag{5}$$

where q_e is the amount of NaCl adsorbed at equilibrium, q_m is the maximum adsorption capacity, C_e represents the equilibrium concentration, and K_L is the Langmuir constant related to the sorption energy.

$$\text{Freundlich: } q_e = K_F C_e^{1/n} \tag{6}$$

The linear form of the Freundlich model could be expressed as

$$\log q_e = \frac{1}{n}\log C_e + \log K_F \tag{7}$$

where K_F is a Freundlich constant, which indicates the relative adsorption capacity of the adsorbent, and $1/n$ is the heterogeneity factor representing the deviation from linearity of adsorption and is also known as the Freundlich coefficient.[68]

Parameters of Gr−Cs−Mn_3O_4 electrode for Langmuir and Freundlich isotherms are shown in Table S3. We can see that the values of r, which is the correlation coefficient of the linear regressions derived from the linear regressions of the Freundlich equation, is larger than that from the linear regressions of Langmuir equation. The Freundlich adsorption equation is derived from Henry's law, which is obtained under conditions of low concentrations of solute.[69] Furthermore, the Freundlich constant $1/n$ is smaller than 1, which is a favorable process. It can be attributed to the molecular interaction between adsorbents and the adsorbates.[47] Thus, all the results demonstrated that the Freundlich equation can better fit the electrosorption curves of the Gr−Cs−Mn_3O_4 electrode.

CONCLUSIONS

We have demonstrated a facile approach to prepare Gr−Cs and Gr−Cs−Mn_3O_4 xerogels by incorporation of chitosan and Mn_3O_4 into graphene sheets. First, Gr−Cs xerogels prepared by the noncovalent interactions possess high adsorption capacities of heavy metal ions. Subsequently, uniform distribution of Mn_3O_4 plus the porous conductive graphene network can be obtained with the aid of high-temperature processing. The synergistic effect of the high capacitance of Mn_3O_4 coating and the porosity left by chitosan offers Gr−Cs−Mn_3O_4 hybrids a superior electrochemical performance with good cycling stability and low inner resistance. The enhanced electrochemical properties of the Gr−Cs−Mn_3O_4 electrodes lead to an outstanding specific electrosorptive capacity of 12.7 mg/g, which is much higher than a pure pristine Gr electrode. We expect that Gr−Cs−Mn_3O_4 composites prepared by this green method will facilitate the fabrication of suitable and promising materials for high-performance CDI electrodes.

DOI: 10.1021/acssuschemeng.5b00193
ACS Sustainable Chem. Eng. 2015, 3, 1056−1065

■ ASSOCIATED CONTENT

Supporting Information

The characterizations of the Gr−Cs−PbO, Gr−Cs−NiO, and Gr−Cs−Mn_3O_4 composites, including optical photograph, XPS spectra, N_2 adsorption/desorption, and FT-IR spectrum. The CV curves and Nyquist plots of the EIS for Gr, Gr−Cs−PbO, and Gr−Cs−NiO by the three-electrode configuration test. The Supporting Information is available free of charge on the ACS Publications website at DOI: 10.1021/acssuschemeng.5b00193.

■ AUTHOR INFORMATION

Corresponding Author

*Tel. & Fax: +86-20-22236269. E-mail: zhywang@scut.edu.cn.

Notes

The authors declare no competing financial interest.

■ ACKNOWLEDGMENTS

This work was financially supported by the National Natural Science Foundation of China (21274046 and 21474032), the National Natural Basic Research Program of China (973 Program, 2012CB821500) and the Natural Science Foundation of Guangdong Province (S2012020011057).

■ REFERENCES

(1) Oren, Y. Capacitive deionization (CDI) for desalination and water treatment - past, present and future (a review). *Desalination* **2008**, *228*, 10−29.

(2) Li, M. Z.; Chen, Y. Z.; Huang, Z. H.; Kang, F. Y. Asymmetric electrodes constructed with PAN-based activated carbon fiber in capacitive deionization. *J. Nanomater.* **2014**, *2014*, 1−6.

(3) AlMarzooqi, F. A.; Al Ghaferi, A. A.; Saadat, I.; Hilal, N. Application of Capacitive Deionisation in water desalination: A review. *Desalination* **2014**, *342*, 3−15.

(4) Dreyer, D. R.; Park, S.; Bielawski, C. W.; Ruoff, R. S. The chemistry of graphene oxide. *Chem. Soc. Rev.* **2010**, *39*, 228−240.

(5) Wen, X. R.; Zhang, D. S.; Yan, T. T.; Zhang, J. P.; Shi, L. Y. Three-dimensional graphene-based hierarchically porous carbon composites prepared by a dual-template strategy for capacitive deionization. *J. Mater. Chem. A* **2013**, *1*, 12334−12344.

(6) Haro, M.; Rasines, G.; Macias, C.; Ania, C. O. Stability of a carbon gel electrode when used for the electro-assisted removal of ions from brackish water. *Carbon* **2011**, *49*, 3723−3730.

(7) Oschatz, M.; Borchardt, L.; Thommes, M.; Cychosz, K. A.; Gogotsi, Y.; Kaskel, S. Carbide-derived carbon monoliths with hierarchical pore architectures. *Angew. Chem., Int. Ed.* **2012**, *51*, 7577−7580.

(8) Li, H. B.; Gao, Y.; Pan, L. K.; Zhang, Y. P.; Chen, Y. W.; Sun, Z. Electrosorptive desalination by carbon nanotubes and nanofibres electrodes and ion-exchange membranes. *Water Res.* **2008**, *42*, 4923−4928.

(9) Lin, Z. Y.; Li, Z.; Moon, K. S.; Fang, Y. N.; Yao, Y. G.; Li, L. Y.; Wong, C. P. Robust vertically aligned carbon nanotube−carbon fiber paper hybrid as versatile electrodes for supercapacitors and capacitive deionization. *Carbon* **2013**, *63*, 547−553.

(10) Dong, Q.; Wang, G.; Qian, B. Q.; Hu, C.; Wang, Y. W.; Qiu, J. S. Electrospun composites made of reduced graphene oxide and activated carbon nanofibers for capacitive deionization. *Electrochim. Acta* **2014**, *137*, 388−394.

(11) Shi, K. Y.; Ren, M.; Zhitomirsky, I. Activated carbon-coated carbon nanotubes for energy storage in supercapacitors and capacitive water purification. *ACS Sustainable Chem. Eng.* **2014**, *2*, 1289−1298.

(12) Shi, K. Y.; Zhitomirsky, I. Supercapacitor devices for energy storage and capacitive dye removal from aqueous solutions. *RSC Adv.* **2015**, *5*, 320−327.

(13) Zhang, D. S.; Yan, T. T.; Shi, L. Y.; Peng, Z.; Wen, X. R.; Zhang, J. P. Enhanced capacitive deionization performance of graphene/carbon nanotube composites. *J. Mater. Chem.* **2012**, *22*, 14696−14704.

(14) Yang, Z. Y.; Jin, L. J.; Lu, G. Q.; Xiao, Q. Q.; Zhang, Y. X.; Jing, L.; Zhang, X. X.; Yan, Y. M.; Sun, K. N. Sponge-templated preparation of high surface area graphene with ultrahigh capacitive deionization performance. *Adv. Funct. Mater.* **2014**, *24*, 3917−3925.

(15) Wang, H.; Shi, L. Y.; Yan, T. T.; Zhang, J. P.; Zhong, Q. D.; Zhang, D. S. Design of graphene-coated hollow mesoporous carbon spheres as high performance electrodes for capacitive deionization. *J. Mater. Chem. A* **2014**, *2*, 4739−4750.

(16) Yan, C. J.; Kanaththage, Y. W.; Short, R.; Gibson, C. T.; Zou, L. Graphene/Polyaniline nanocomposite as electrode material for membrane capacitive deionization. *Desalination* **2014**, *344*, 274−279.

(17) Peng, Z.; Zhang, D. S.; Yan, T. T.; Zhang, J. P.; Shi, L. Y. Three-dimensional micro/mesoporous carbon composites with carbon nanotube networks for capacitive deionization. *Appl. Surf. Sci.* **2013**, *282*, 965−973.

(18) Peng, Z.; Zhang, D. S.; Shi, L. Y.; Yan, T. T. High performance ordered mesoporous carbon/carbon nanotube composite electrodes for capacitive deionization. *J. Mater. Chem.* **2012**, *22*, 6603−6612.

(19) Lei, H.; Yan, T. T.; Wang, H.; Shi, L. Y.; Zhang, J. P.; Zhang, D. S. Graphene-like carbon nanosheets prepared by a Fe-catalyzed glucose-blowing method for capacitive deionization. *J. Mater. Chem. A* **2015**, *3*, 5934−5941.

(20) Zhang, D. S.; Wen, X. R.; Shi, L. Y.; Yan, T. T.; Zhang, J. P. Enhanced capacitive deionization of graphene/mesoporous carbon composites. *Nanoscale* **2012**, *4*, 5440−5446.

(21) Ni, Z. H.; Yu, T.; Lu, Y. H.; Wang, Y. Y.; Feng, Y. P.; Shen, Z. X. Uniaxial strain on graphene: Raman spectroscopy study and band-gap opening. *ACS Nano* **2008**, *2*, 2301−2305.

(22) Lv, W.; You, C. H.; Wu, S. D.; Li, B. H.; Zhu, Z. P.; Wang, M. Z.; Yang, Q. H.; Kang, F. Y. pH-Mediated fine-tuning of optical properties of graphene oxide membranes. *Carbon* **2012**, *50*, 3233−3239.

(23) Zhang, H. B.; Zheng, W. G.; Yan, Q. Y.; Jiang, Z. G.; Yu, Z. Z. The effect of surface chemistry of graphene on rheological and electrical properties of polymethylmethacrylate composites. *Carbon* **2012**, *50*, 5117−5125.

(24) Lo, C. W.; Zhu, D. F.; Jiang, H. R. An infrared-light responsive graphene-oxide incorporated poly(N-isopropylacrylamide) hydrogel nanocomposite. *Soft Matter* **2011**, *7*, 5604−5609.

(25) Yang, Y.; Ren, L. L.; Zhang, C.; Huang, S.; Liu, T. X. Facile fabrication of functionalized graphene sheets (FGS)/ZnO nanocomposites with photocatalytic property. *ACS Appl. Mater. Interfaces* **2011**, *3*, 2779−2785.

(26) Bi, H.; Sun, S. R.; Huang, F. Q.; Xie, X. M.; Jiang, M. H. Direct growth of few-layer graphene films on SiO_2 substrates and their photovoltaic applications. *J. Mater. Chem.* **2012**, *22*, 411−416.

(27) Han, W. J.; Ren, L.; Gong, L. J.; Qi, X.; Liu, Y. D.; Yang, L. W.; Wei, X. L.; Zhong, J. X. Self-assembled three-dimensional graphene-based aerogel with embedded multifarious functional nanoparticles and its excellent photoelectrochemical activities. *ACS Sustainable Chem. Eng.* **2014**, *2*, 741−748.

(28) Wang, B.; Park, J. S.; Wang, C. Y.; Ahn, H. J.; Wang, G. X. Mn_3O_4 nanoparticles embedded into graphene nanosheets: Preparation, characterization, and electrochemical properties for supercapacitors. *Electrochim. Acta* **2010**, *55*, 6812−6817.

(29) Liu, Y. T.; Feng, Q. P.; Xie, X. M.; Ye, X. Y. The production of flexible and transparent conductive films of carbon nanotube/graphene networks coordinated by divalent metal (Cu, Ca or Mg) ions. *Carbon* **2011**, *49*, 3371−3375.

(30) Qian, W.; Greaney, P. A.; Fowler, S.; Chiu, S. K.; Goforth, A. M.; Jiao, J. Low-temperature nitrogen doping in ammonia solution for production of N-doped TiO_2-hybridized graphene as a highly efficient photocatalyst for water treatment. *ACS Sustainable Chem. Eng.* **2014**, *2*, 1802−1810.

(31) Kalpana, K. V.; Selvan, R. K. Electrochemical properties of microwave-assisted reflux-synthesized Mn_3O_4 nanoparticles in differ-

DOI: 10.1021/acssuschemeng.5b00193
ACS Sustainable Chem. Eng. 2015, 3, 1056−1065

ent electrolytes for supercapacitor applications. *J. Appl. Electrochem.* **2012**, *42*, 463−470.
(32) Liu, M. K.; Tjiu, W. W.; Pan, J. S.; Zhang, C.; Gao, W.; Liu, T. X. One-step synthesis of graphene nanoribbon-MnO_2 hybrids and their all-solid-state asymmetric supercapacitors. *Nanoscale* **2014**, *6*, 4233−4242.
(33) Li, L.; Seng, K. H.; Chen, Z. X.; Liu, H. K.; Nevirkovets, I. P.; Guo, Z. P. Synthesis of Mn_3O_4-anchored graphene sheet nanocomposites via a facile, fast microwave hydrothermal method and their supercapacitive behavior. *Electrochim. Acta* **2013**, *87*, 801−808.
(34) Wu, Y. Z.; Liu, S. Q.; Wang, H. Y.; Wang, X. W.; Zhang, X.; Jin, G. H. A novel solvothermal synthesis of Mn_3O_4/graphene composites for supercapacitors. *Electrochim. Acta* **2013**, *90*, 210−218.
(35) Liu, H.; Wang, C. Y. Chitosan scaffolds for recyclable adsorption of Cu(ii) ions. *RSC Adv.* **2014**, *4*, 3864−3872.
(36) Qian, L.; Zhang, H. F. Green synthesis of chitosan-based nanofibers and their applications. *Green Chem.* **2010**, *12*, 1207−1214.
(37) Han, D.; Yan, L. Supramolecular hydrogel of chitosan in the presence of graphene oxide nanosheets as 2D cross-linkers. *ACS Sustainable Chem. Eng.* **2014**, *2*, 296−300.
(38) Shao, L.; Chang, X. J.; Zhang, Y. L.; Huang, Y. F.; Yao, Y. H.; Guo, Z. H. Graphene oxide cross-linked chitosan nanocomposite membrane. *Appl. Surf. Sci.* **2013**, *280*, 989−992.
(39) Bora, C.; Dolui, S. K. Fabrication of polypyrrole/graphene oxide nanocomposites by liquid/liquid interfacial polymerization and evaluation of their optical, electrical and electrochemical properties. *Polymer* **2012**, *53*, 923−932.
(40) Fan, L. L.; Luo, C. N.; Sun, M.; Li, X. J.; Qiu, H. M. Highly selective adsorption of lead ions by water-dispersible magnetic chitosan/graphene oxide composites. *Colloid Surface B* **2013**, *103*, 523−529.
(41) Fan, L. L.; Luo, C. N.; Li, X. J.; Lu, F. G.; Qiu, H. M.; Sun, M. Fabrication of novel magnetic chitosan grafted with graphene oxide to enhance adsorption properties for methyl blue. *J. Hazard. Mater.* **2012**, *215−216*, 272−279.
(42) Gu, X. Y.; Ning, Y.; Yang, Y.; Wang, C. Y. One-step synthesis of porous graphene-based hydrogels containing oil droplets for drug delivery. *RSC Adv.* **2014**, *4*, 3211−3218.
(43) Chen, Y. Q.; Chen, L. B.; Bai, H.; Li, L. Graphene oxide−chitosan composite hydrogels as broad-spectrum adsorbents for water purification. *J. Mater. Chem. A* **2013**, *1*, 1992−2001.
(44) Kim, Y. J.; Choi, J. H. Improvement of desalination efficiency in capacitive deionization using a carbon electrode coated with an ion-exchange polymer. *Water Res.* **2010**, *44*, 990−996.
(45) Jia, B. P.; Zou, L. Graphene nanosheets reduced by a multi-step process as high-performance electrode material for capacitive deionisation. *Carbon* **2012**, *50*, 2315−2321.
(46) Ji, C. C.; Xu, M. W.; Bao, S. J.; Cai, C. J.; Lu, Z. J.; Chai, H.; Yang, F.; Wei, H. Self-assembly of three-dimensional interconnected graphene-based aerogels and its application in supercapacitors. *J. Colloid Interface Sci.* **2013**, *407*, 416−424.
(47) Li, L. L.; Fan, L. L.; Sun, M.; Qiu, H. M.; Li, X. J.; Duan, H. M.; Luo, C. N. Adsorbent for hydroquinone removal based on graphene oxide functionalized with magnetic cyclodextrin-chitosan. *Int. J. Biol. Macromol.* **2013**, *58*, 169−175.
(48) Zhang, L.; Shi, G. Q. Preparation of highly conductive graphene hydrogels for fabricating supercapacitors with high rate capability. *J. Phys. Chem. C* **2011**, *115*, 17206−17212.
(49) Zhao, G. X.; Li, J. X.; Ren, X. M.; Chen, C. L.; Wang, X. K. Few-layered graphene oxide nanosheets as superior sorbents for heavy metal ion pollution management. *Environ. Sci. Technol.* **2011**, *45*, 10454−10462.
(50) Fu, Y.; Wang, J. Y.; Liu, Q. X.; Zeng, H. B. Water-dispersible magnetic nanoparticle−graphene oxide composites for selenium removal. *Carbon* **2014**, *77*, 710−721.
(51) Gollavelli, G.; Chang, C. C.; Ling, Y. C. Facile synthesis of smart magnetic graphene for safe drinking water: heavy metal removal and disinfection control. *ACS Sustainable Chem. Eng.* **2013**, *1*, 462−472.
(52) Whitby, R. L. D. Chemical control of graphene architecture: tailoring shape and properties. *ACS Nano* **2014**, *8*, 9733−9754.
(53) Liu, L.; Li, C.; Bao, C.; Jia, Q.; Xiao, P.; Liu, X.; Zhang, Q. Preparation and characterization of chitosan/graphene oxide composites for the adsorption of Au(III) and Pd(II). *Talanta* **2012**, *93*, 350−357.
(54) Lee, J. W.; Hall, A. S.; Kim, J.-D.; Mallouk, T. E. A facile and template-free hydrothermal synthesis of Mn_3O_4 nanorods on graphene sheets for supercapacitor electrodes with long cycle stability. *Chem. Mater.* **2012**, *24*, 1158−1164.
(55) Zhu, L. X.; Zhang, S.; Cui, Y. H.; Song, H. H.; Chen, X. H. One step synthesis and capacitive performance of graphene nanosheets/Mn3O4 composite. *Electrochim. Acta* **2013**, *89*, 18−23.
(56) Lee, D. H.; Kim, J. C.; Shim, H. W.; Kim, D. W. Highly reversible Li storage in hybrid NiO/Ni/graphene nanocomposites prepared by an electrical wire explosion process. *ACS Appl. Mater. Interfaces* **2014**, *6*, 137−142.
(57) Hwang, S. G.; Kim, G. O. K.; Yun, S. R.; Ryu, K. S. NiO nanoparticles with plate structure grown on graphene as fast charge−discharge anode material for lithium ion batteries. *Electrochim. Acta* **2012**, *78*, 406−411.
(58) Aliakbari, A.; Najafi, E.; Amini, M. M.; Ng, S. W. Structure and photoluminescence properties of lead(II) oxide nanoparticles synthesized from a new lead(II) coordination polymer. *Monatsh. Chem.* **2014**, *145*, 1277−1285.
(59) Cao, X. H.; Shi, Y. M.; Shi, W. H.; Lu, G.; Huang, X.; Yan, Q. Y.; Zhang, Q. C.; Zhang, H. Preparation of novel 3D graphene networks for supercapacitor applications. *Small* **2011**, *7*, 3163−3168.
(60) Zafra, M. C.; Lavela, P.; Rasines, G.; Macías, C.; Tirado, J. L.; Ania, C. O. A novel method for metal oxide deposition on carbon aerogels with potential application in capacitive deionization of saline water. *Electrochim. Acta* **2014**, *135*, 208−216.
(61) Yin, H. J.; Zhao, S. L.; Wan, J. W.; Tang, H. J.; Chang, L. C.; He, L.; Zhao, H. J.; Gao, Y.; Tang, Z. Y. Three-dimensional graphene/metal oxide nanoparticle hybrids for high-performance capacitive deionization of saline water. *Adv. Mater.* **2013**, *25*, 6270−6276.
(62) Cai, P. F.; Su, C. J.; Chang, W. T.; Chang, F. C.; Peng, C. Y.; Sun, I. W.; Wei, Y. L.; Jou, C. J.; Wang, H. P. Capacitive deionization of seawater effected by nano Ag and Ag@C on graphene. *Mar. Pollut. Bull.* **2014**, *85*, 733−737.
(63) Jeon, S.; Park, H.; Yeo, J.; Yang, S. C.; Cho, C. H.; Han, M. H.; Kim, D. K. Desalination via a new membrane capacitive deionization process utilizing flow-electrodes. *Energy Environ. Sci.* **2013**, *6*, 1471−1475.
(64) Li, H. B.; Liang, S.; Li, J.; He, L. J. The capacitive deionization behaviour of a carbon nanotube and reduced graphene oxide composite. *J. Mater. Chem. A* **2013**, *1*, 6335−6341.
(65) Wang, G.; Qian, B. Q.; Dong, Q.; Yang, J. Y.; Zhao, Z. B.; Qiu, J. S. Highly mesoporous activated carbon electrode for capacitive deionization. *Sep. Purif. Technol.* **2013**, *103*, 216−221.
(66) Xu, P.; Drewes, J. E.; Heil, D.; Wang, G. Treatment of brackish produced water using carbon aerogel-based capacitive deionization technology. *Water Res.* **2008**, *42*, 2605−2617.
(67) Lee, J. B.; Park, K. K.; Eum, H. M.; Lee, C. W. Desalination of a thermal power plant wastewater by membrane capacitive deionization. *Desalination* **2006**, *196*, 125−134.
(68) Wu, Y.; Luo, H. J.; Wang, H.; Wang, C.; Zhang, J.; Zhang, Z. L. Adsorption of hexavalent chromium from aqueous solutions by graphene modified with cetyltrimethylammonium bromide. *J. Colloid Interface Sci.* **2013**, *394*, 183−191.
(69) Li, H. B.; Lu, T.; Pan, L. K.; Zhang, Y. P.; Sun, Z. Electrosorption behavior of graphene in NaCl solutions. *J. Mater. Chem.* **2009**, *19*, 6773−6779.

DOI: 10.1021/acssuschemeng.5b00193
ACS Sustainable Chem. Eng. 2015, 3, 1056−1065